*International Journal of Minerals, Metallurgy and Materials*
*Volume 26, Number 2, February 2019, Page 210*
**https://doi.org/10.1007/s12613-019-1726-8**

# Development of gas tungsten arc welding using current pulsing technique to preclude chromium carbide precipitation in aerospace-grade alloy 80A

*P. Subramani and M. Manikandan*

School of Mechanical Engineering, Vellore Institute of Technology, Vellore 632014, India
(Received: 2 May 2018; revised: 28 June 2018; accepted: 13 July 2018)

**Abstract:** Weldments were produced using gas tungsten arc welding (GTAW) and pulsed current gas tungsten arc welding (PCGTAW) techniques with ERNiCr-3 filler wire. Macro examination revealed that the resultant weldments were free from defects. A refined microstructure was observed in the weldment fabricated through PCGTAW. Scanning electron microscopy (SEM) analysis revealed secondary phases in the grain boundaries. Energy-dispersive X-ray spectroscopy (EDS) analysis revealed that microsegregation of Cr carbide precipitates was completely eradicated through PCGTAW. The microsegregation of Nb precipitates was observed in the GTA and PCGTA weldments. X-ray diffraction (XRD) analysis revealed the existence of $M_{23}C_6$ Cr-rich carbide and $Ni_8Nb$ phases in the GTA weldments. By contrast, in the PCGTA weldments, the $Ni_8Nb$ phase was observed. The $Cr_2Ti$ phase was observed in both the GTA and the PCGTA weldments. Tensile tests showed that the strength and ductility of the PCGTA weldments were slightly higher than those of the GTA weldments.

**Keywords:** Ni-based superalloy; welding; pulse current; microsegregation; chromium carbide

## 1. Introduction

Alloy 80A (UNS N07080 (ASTM B637-06)) is an age-hardened Ni-based superalloy derived from the Ni–Cr system. It is a precipitation-strengthened alloy developed for service at temperatures as high as of 815°C [1]. The manufacturing process of alloy 80A comprises solid strengthening of the alloy with the γ matrix phase, followed by precipitation strengthening of the alloy with a γ′ matrix phase. The precipitation strengthening is carried out by adding small amounts of Ti and Al to the metal matrix of the alloy to form strengthening phases such as $Ni_3Al$, $Ni_3Ti$, and $Ni_3(Al,Ti)$ [2]. Alloy 80A is designed for aerospace applications such gas turbine components (rings, blades, and discs). It is also used in nuclear power plants in components such as bolts and boiler tube supports and in automobile internal combustion engines as exhaust valves [1,3]. Less attention has been devoted to alloy 80A than to other Ni-based superalloys because it is less readily available [3].

Arc welding is commercially used in many industries for joining metallic components. Gas tungsten arc welding (GTAW) is an arc welding technique commercially used to join Ni–Cr alloys. However, in most cases, GTAW of Ni–Cr alloy leads to the problems of hot cracking and the formation of $M_{23}C_6$ ($Cr_{23}C_6$) carbide precipitates around grain boundaries [4–5]. Hot cracking and $M_{23}C_6$ carbide precipitation around the grain boundaries in the weld bead tend to deteriorate the mechanical properties of the alloy [5–6]. Thus, an investigation of the weld behavior of alloy 80A fabricated through the GTAW technique is warranted.

GTAW of alloy 80A leads to poor-quality welds because of weldment hot cracking caused by the agglomeration of $Cr_{23}C_6$ carbide and the depletion of Cr around the grain boundaries [4–6]. Keienburg *et al.* [6] studied the renovation of an alloy 80A turbine blade. They reported that when the blade had been refurbished through GTAW with Inconel 62 filler wire, large cracks were observed in the weld-bead interface region of the fusion zone (FZ). The observed large cracks were reduced to microcracks when a piece of Inconel 625 was placed over the alloy 80A using GTAW with Inconel 625 filler wire. Kargarnejad and Djavanroodi [7] studied the cause of failure of an alloy 80A turbine blade. They reported that, when the turbine blade was exposed to high temperatures, a continuous film of carbides was identified in

Corresponding author: M. Manikandan E-mail: mano.manikandan@gmail.com; rubeshpsm@gmail.com
© University of Science and Technology Beijing and Springer-Verlag GmbH Germany, part of Springer Nature 2019

the grain boundaries, where it increased the transformation of MC-type carbides to 88% $M_{23}C_6$ (Cr-rich precipitate) + 22% coarsened γ′ phase during service. The presence of $M_{23}C_6$ carbides and the coarsening of γ′ phases are detrimental to high-temperature creep property of alloy 80A. Gao and Wei [8] and Xu *et al.* [9] studied the microstructural changes of alloy 80A exposed to different treatments and reported that segregated $M_{23}C_6$ Cr-rich carbide phases formed in the grain boundaries of the alloy. These authors noted that blocky $M_{23}C_6$ Cr-rich carbides tended to adversely affect the mechanical properties of the alloy.

According to the literature, the presence of segregated Cr carbides around grain boundaries is detrimental to the mechanical properties of alloy 80A. This problem can be eradicated by the selection of an appropriate welding technique, proper processing parameters, and filler wire. In the present research work, welding of alloy 80A is conducted through GTAW and pulsed current gas tungsten arc welding (PCGTAW) modes with ERNiCr-3 filler wire. The ERNiCr-3 filler wire is recommended for welding of alloy 80A by manufacturer ThyssenKrupp [10]. The chemical composition of ERNiCr-3 filler wire is nearly the same as that of alloy 80A, except for the addition of a substantial amount of Nb in the metal matrix. The use of the PCGTAW technique in the welding of alloy 80A is expected to suppress or reduce the problem of microsegregation of alloying elements around grain boundaries. A review of the literature suggests that the PCGTAW technique should be beneficial in suppressing the microsegregation of alloy 80A.

Ram *et al.* [11] reported a reduction of laves-phase formation in weldments of alloy 718. They claimed that, with implementation of a current pulsing mode, the formation of laves phase and Nb segregation were reduced. Thus, a reduction in laves-phase formation and Nb segregation could improve the stress rupture property of the weld joint. Manikandan *et al.* [12] studied the influence of cooling rate on the precipitation of alloying elements in the weld zone of alloy 718. They reported that using the current pulsing mode resulted in the maximum cooling rate and was helpful in minimizing the precipitation of alloying elements in the weldment. Our group [13] also reported comparative studies between the GTAW and PCGTAW of alloy 686. We found that switching from the GTAW to the PCGTAW technique reduced microsegregation of the alloying elements and thereby enhanced the mechanical properties of the weld joints. Similar results have been reported in other studies [14–15].

Ramkumar *et al.* [16] reported the influence of the PCGTAW technique on the structural and mechanical properties of alloy X750 weld joints fabricated with two different filler wires. They reported that adopting the PCGTAW technique eliminated the segregation of Cr carbide precipitates in the weldment and that the reduced microsegregation resulted in weld joints with good mechanical properties.

We [17] studied the effect of the GTAW and PCGTAW techniques on sensitization in weldments fabricated with three different filler wires and found that switching from GTA to PCGTA welding eliminated the formation of the $M_{23}C_6$ carbide phase. We also observed a weld bead with good morphology and a refined microstructure in the PCGTA weldments. The application of the PCGTAW technique to Ni–Cr alloys such as alloys X750 and 600 reduced or eliminated the microsegregation of alloying elements in the weld beads. Because alloy 80A is also derived from the Ni–Cr system, we expected similar results in the current study.

On the basis of our review of the literature, a suitable arc welding technique should be developed for welding alloy 80A. Thus far, the literature contains no reports of the welding of alloy 80A using the GTAW or PCGTAW technique with ERNiCr-3 filler wire. The aim of the current study is to assess the welding characteristics of alloy 80A and to reduce the microsegregation of alloying elements in the grain boundaries. The improvement attained in the welding of alloy 80A through the PCGTA welding technique is reported herein. We expect that the knowledge gained in the present work can be utilized in industry to obtain defect-free welds.

## 2. Experimental

### 2.1. Materials and welding procedure

Alloy 80A was acquired as a solution-annealed material in the form of a 6-mm-thick plate. The alloy 80A was subjected to elemental analysis by optical emission spectroscopy. The results are listed in Table 1.

Before the welding trials were carried out, the acquired plate was machined to dimensions of 170 mm × 50 mm × 6 mm using an electrical discharge machining process. The machined plates were subjected to acid pickling to remove strain and impurities such as rust, followed by cleaning with acetone to remove markings, dirt, and oil from the plates prior to the welding process. Before the welding process,

**Table 1. Chemical compositions of alloy 80A and filler wire ERNiCr-3** wt%

| Base/filler wire | Ni | Cr | Fe | Mn | Al | Ti | Others |
|---|---|---|---|---|---|---|---|
| Alloy 80A | Bal. | 20.53 | 0.042 | 0.357 | 1.59 | 2.48 | 0.010 (S), 0.142 (Si), 0.073 (C) |
| ERNiCr-3 | Bal. | 19.59 | 0.751 | 2.95 | 0.27 | 0.43 | 2.424 (Nb), 0.38 (Si) |

standard V-grooves with an included angle of 45° were made in the plates. The machined plates were clamped to fixtures to avoid bending during welding. Manual welding was carried out on plates in both GTAW and PCGTAW modes using a KEMPI DWE 400 AC/DC machine. The weldments were fabricated using ERNiCr-3 filler wire by melting and filling the groove. The composition of the ERNiCr-3 filler wire is also given in Table 1. To avoid contamination by impurities in the molten region of the weld bead, argon was used as a shielding gas during welding, with a flow rate of 15 L/min. During welding, oxide layers formed over the weld bead were removed using a wire brush after each pass. The process parameters employed in the present study to fabricate GTA and PCGTA weldments are shown in Table 2.

**Table 2. Welding process parameter used in GTA and PCGTA welded joints with ERNiCr-3 filler wire**

| Type of welding | Filler wire diameter / mm | No. of pass | Current / A | Voltage / V | Welding speed / (mm·s$^{-1}$) | Heat input / (kJ·mm$^{-1}$) | Total heat input / (kJ·mm$^{-1}$) |
|---|---|---|---|---|---|---|---|
| GTA | 1.6 | Root | 120 | 9.4 | 1.30 | 0.608 | 2.052 |
| | | First | 120 | 9.4 | 1.00 | 0.789 | |
| | | Second | 120 | 9.4 | 1.21 | 0.654 | |
| PCGTA | 1.6 | Root | $I_p$ 120, $I_b$ 66 | 8.9 | 1.04 | 0.555 | 1.809 |
| | | First | $I_p$ 120, $I_b$ 66 | 8.9 | 1.06 | 0.545 | |
| | | Second | $I_p$ 120, $I_b$ 66 | 8.9 | 1.53 | 0.378 | |
| | | Third | $I_p$ 120, $I_b$ 66 | 8.9 | 1.75 | 0.330 | |

Note: $I_b$ is the background current; $I_p$ is the pulse current.

The welding heat input during each pass was calculated for both the GTAW and PCGTAW processes; the results are tabulated in Table 2. For the GTAW process, a constant current was used in the calculation of the heat input; by contrast, for the PCGTAW process, the mean current ($I_m$, A) was utilized.

In GTAW, the heat input (HI, kJ/mm) is derived using the equation

$$\mathrm{HI} = \eta \times \frac{I_m \times V}{S} \quad (1)$$

In the case of PCGTAW, HI is derived using the following equations:

$$I_m = \frac{I_P \times t_p + I_b \times t_b}{t_p + t_b} \quad (2)$$

$$\mathrm{HI} = \eta \times \frac{I_m \times V}{S} \quad (3)$$

where $I_b$ is the background current (A); $I_p$ is the pulse current (A); $t_p$ is the duration of the pulse current (ms); $t_b$ is the duration of the background current (ms); $V$ is the voltage (V); $S$ is the welding speed (mm/min); and $\eta$ is the efficiency of the welding (70% for both GTAW and PCGTAW) [13,17].

## 2.2. Metallurgical and mechanical examinations

Welding was carried out in the direction perpendicular to the rolling direction. Fig. 1 shows photographs of the weldments fabricated by GTAW and PCGTAW.

Weld coupons were extracted in the direction perpendicular to the weld direction. The cross-section of the weld joint was used for metallurgical examination; it comprises (1) the base metal (BM), (2) the heat-affected zone (HAZ), and (3) the FZ. The extracted coupons were mounted using black light powder in a hot-press mounting machine. Samples were polished in two steps: first step with SiC emery sheets (220 to 2000 grit size) polishing, and then second step with alumina + water polishing, and finished with only water polishing to obtain a mirror-like smooth surface. The polished samples were then exposed to electrolytic etching in 10wt% chromic acid solution in 100 mL of water for 4–5 s to reveal the microstructure. To determine the traces of defects in the weldments, macro examination was conducted on the transverse section of the FZ. The FZ region of the weldments was observed by optical microscopy and scanning electron

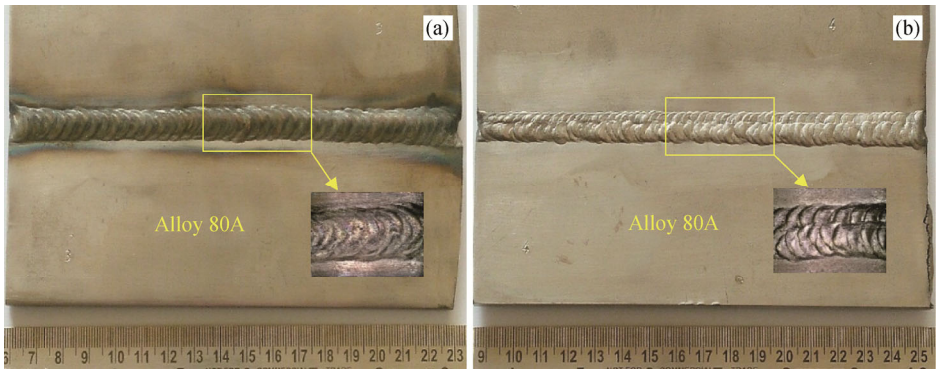


**Fig. 1. Photographs of weldments fabricated with ERNiCr-3 filler wire: (a) GTAW; (b) PCGTAW.**

microscopy (SEM) to observe changes in the microstructure of the weldment in comparison with the microstructure of the alloy 80A. Energy-dispersive X-ray spectroscopy (EDS) was conducted to analyze the segregation of alloying elements in the dendritic core and interdendritic region of the weld zone. X-ray diffraction (XRD) analysis was conducted to determine the composition of the secondary phases in the weld zone. XRD analysis was also used to determine the refinement in the crystalline grain size of GTA and PCGTA weldments.

### 2.3. Mechanical examination

Weldments were subjected to tensile testing to assess the strength and ductility of the weld joints. In accordance with standard ASTM E8/E8M-13a, tensile samples were extracted from the weldments in the direction perpendicular to the weld bead. The tensile testing was conducted at room temperature using an INSTRON 8801 universal testing machine. To check the reproducibility of the test results, three samples were analyzed. The manner in which the failures occurred in the tensile samples was studied through SEM fractographs.

## 3. Results

### 3.1. Macrostructural examination

Macroscale examinations were conducted to evaluate the FZ defects in the weldments. Figs. 2(a) and 2(b) show macrographic images of the weldments fabricated by the GTAW and PCGTAW techniques with ERNiCr-3 filler wire. A defect-free FZ was observed in all of the weldments. We further deduced that the width of the FZ of the PCGTA weldment was narrower than that of the GTA weldment.

### 3.2. Microstructural examination

3.2.1. Base metal

The BM microstructure reveals a face-centered-cubic austenitic structure with some annealing twins in the grain boundaries. Fig. 3 shows the optical microstructure of the as-acquired alloy 80A.

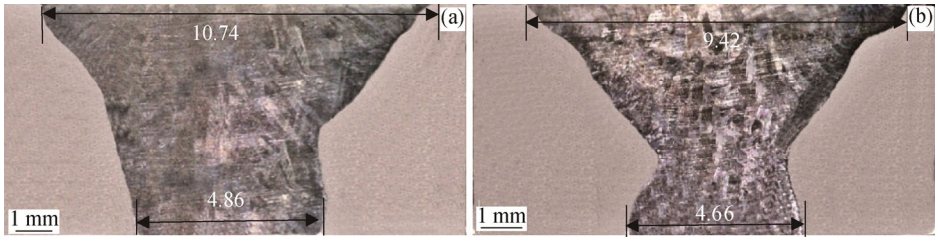


**Fig. 2. Macrographic images of weldments fabricated with ERNiCr-3 filler wire: (a) GTAW; (b) PCGTAW.**

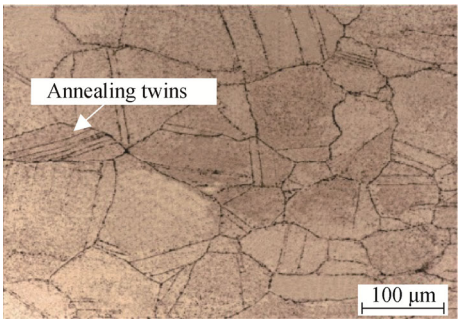


**Fig. 3. Microstructure of the as-acquired alloy 80A.**

3.2.2. GTA and PCGTA weldments with ERNiCr-3 filler wire

Figs. 4 and 5 show the optical microstructures of the GTA and PCGTA weldments of the alloy 80A fabricated with ERNiCr-3 filler wire.

Figs. 4(a) and 4(b) exemplify the microstructure of the FZ weld center and the weld-interface region of the GTA weldment. Figs. 5(a) and 5(b) exemplify the microstructure of the PCGTA weldment. In the GTA weldment, cellular and columnar dendritic structures were observed. By contrast, in the PCGTA weldment, an equiaxed dendritic structure and

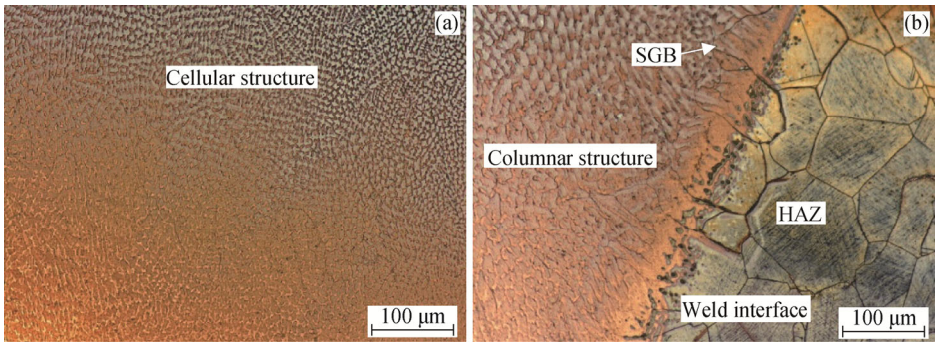


**Fig. 4. Microstructure images of weld joints fabricated by GTAW with ERNiCr-3 filler wire: (a) weld center; (b) weld interface.**

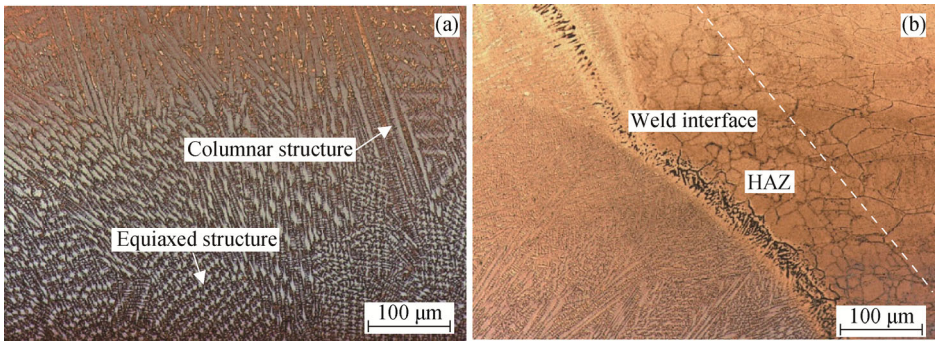


**Fig. 5. Microstructure images of weld joints fabricated by PCGTA with ERNiCr-3 filler wire: (a) weld center; (b) weld interface.**

the columnar dendritic structure were observed. We also found that the grain size is coarser in the HAZ of the GTA weldment and smaller in the HAZ of the PCGTA weldment.

### 3.3. SEM/EDS analysis of GTA and PCGTA weldments with ERNiCr-3 filler wire

Higher-magnification SEM micrographs of the weld center and the weld-interface region of the GTA weldment are shown in Figs. 6(a) and 6(b). Cellular and columnar structures were observed in the FZ weld center and weld-interface regions. Figs. 6(a) and 6(b) shows a secondary-phase precipitate in the interdendritic regions of the FZ.

EDS analysis was conducted in the FZ of the GTA weldment; the results are shown in Figs. 6(c)–6(f). Table 3

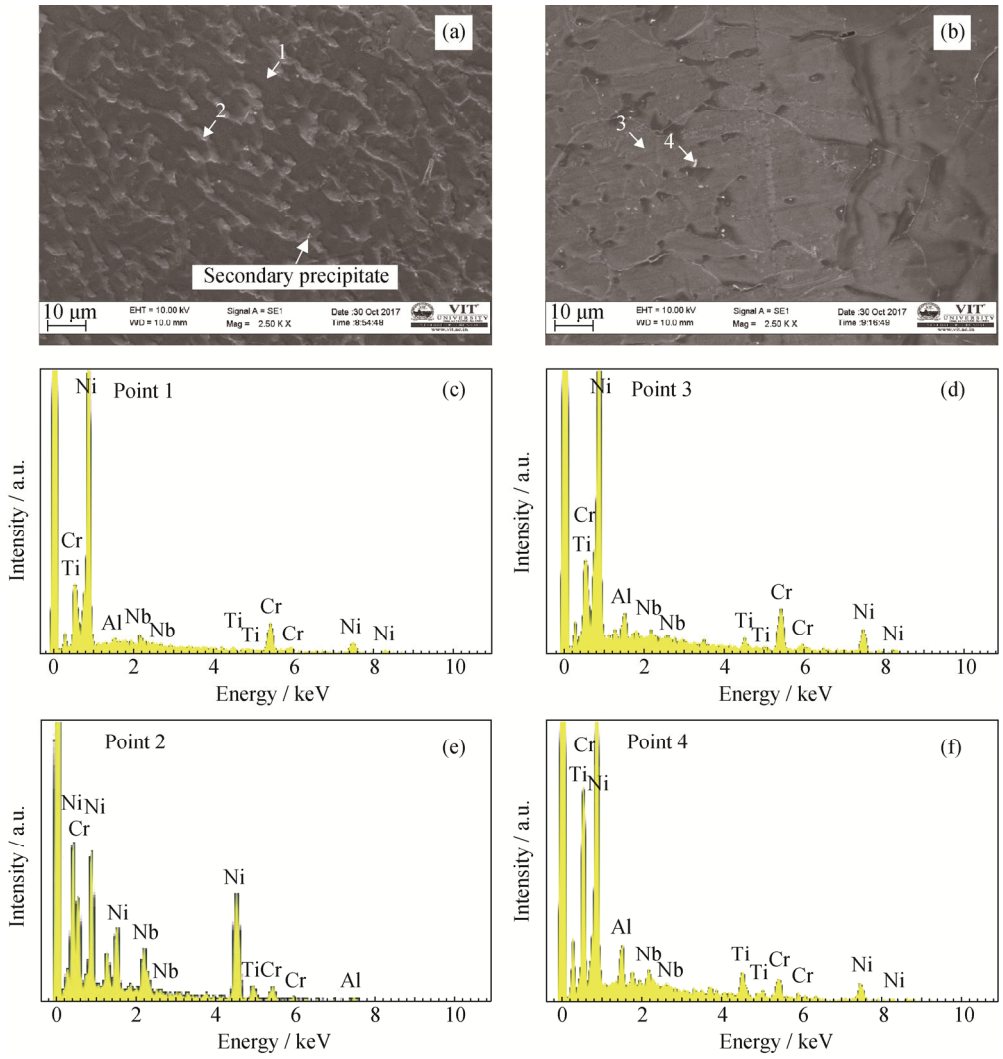


**Fig. 6. SEM/EDS analysis of the GTA–ERNiCr-3 weld joint of alloy 80A: (a) SEM micrograph of the weld center; (b) SEM micrograph of the weld interface; (c) EDS spectrum of the weld-center dendritic core; (d) EDS spectrum of the weld-interface dendritic core; (e) EDS spectrum of the weld-center interdendritic region; (f) EDS spectrum of the weld-interface interdendritic region.**

**Table 3. EDS analysis results at different zones (points 1-4 in Fig. 6) of the GTA weldment with ERNiCr-3** wt%

| Point | Zone | Ni | Cr | Nb | Ti | Al |
|---|---|---|---|---|---|---|
| 1 | Weld-center dendritic core | 70.47 | 26.07 | 2.13 | 0.93 | 0.40 |
| 2 | Weld-center interdendritic region | 46.67 | 45.23 | 5.61 | 1.86 | 0.64 |
| 3 | Weld-interface dendritic core | 73.12 | 22.67 | 2.17 | 1.11 | 0.95 |
| 4 | Weld-interface interdendritic region | 60.66 | 31.82 | 5.82 | 1.07 | 1.38 |

lists the mass percentages of Ni, Cr, Nb, Ti, and Al in the dendritic core and in the interdendritic regions of the weld center and the interface zone of the FZ of the weldments. Figs. 6(c)–6(f) and Table 3 reveal that the interdendritic region is rich in Cr and Nb but poor in Ni. Similar results were obtained for the weld-interface region.

Higher-magnification SEM micrographs of the weld center and weld-interface region of the PCGTA weldment are shown in Figs. 7(a) and 7(b). An equiaxed and columnar structure was observed in the FZ weld center and weld-interface regions. A small amount of secondary-phase precipitate was found in the interdendritic regions in the PCGTA weldment. The results of the EDS analysis of the FZ of the PCGTA weldment are shown in Figs. 7(c)–7(f). Table 4 lists the mass percentage of Ni, Cr, Nb, Ti, and Al at the dendritic core and interdendritic regions of the weld center and interface zone of the FZ of the weldment. Figs. 7(c)–7(f) and Table 4 reveal that the interdendritic region is rich in Nb and Ti compared to its respective dendritic core in both FZ weld center and weld interface region. Similar results were also found in the weld-interface region. We deduced from the results that microsegregation of Cr is

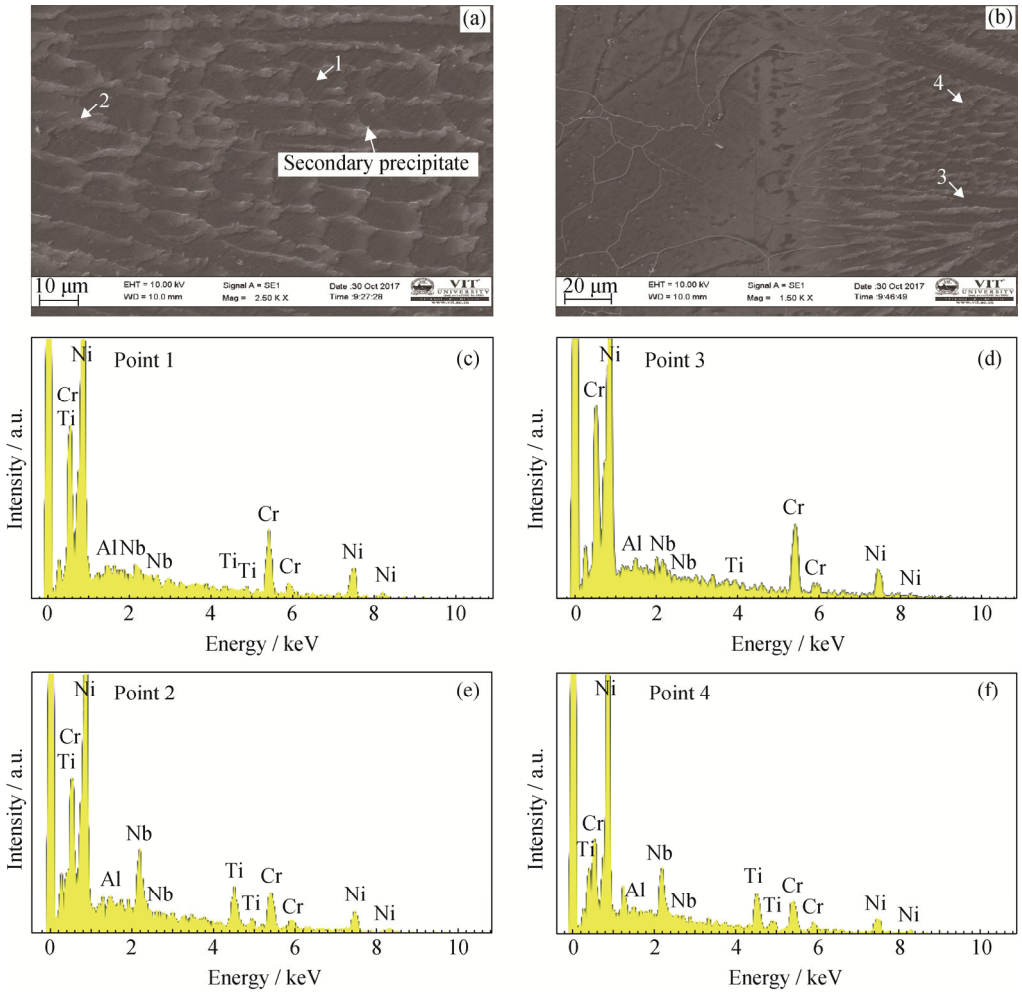


**Fig. 7. SEM/EDS analysis of the PCGTA–ERNiCr-3 weld joint of alloy 80A: (a) SEM micrograph of the weld center; (b) SEM micrograph of the weld interface; (c) EDS spectrum of the weld-center dendritic core; (d) EDS spectrum of the weld-interface dendritic core; (e) EDS spectrum of the weld-center interdendritic region; (f) EDS spectrum of the weld-interface interdendritic region.**

**Table 4. EDS analysis at different zones (points 1–4 in Fig. 7) of PCGTA weldment with ERNiCr-3** wt %

| Point | Zone | Ni | Cr | Nb | Ti | Al |
|---|---|---|---|---|---|---|
| 1 | Weld-center dendritic core | 71.92 | 25.75 | 1.75 | 0.27 | 0.27 |
| 2 | Weld-center interdendritic region | 69.19 | 24.05 | 5.06 | 1.45 | 0.24 |
| 3 | Weld-interface dendritic core | 72.52 | 25.14 | 1.53 | 0.44 | 0.42 |
| 4 | Weld-interface interdendritic region | 70.25 | 22.82 | 5.53 | 1.02 | 0.38 |

completely suppressed in the PCGTA weldments. We also observed microsegregation of Nb in the PCGTA weldments.

### 3.4. XRD analysis

XRD analysis was conducted to assess the presence of a secondary phase in the FZ of the weldments and in the BM. Fig. 8 shows the XRD analysis results. The XRD analysis of the BM reveals the existence of γ′ matrix phase $Ni_3Al$ and $Ni_3(Al,Ti)$. In the GTA weldment with ERNiCrMo-3 filler wire, $Cr_{23}C_6$, $Ni_8Nb$, and $Cr_2Ti$ are observed. In the PCGTA weldment, $Ni_8Nb$, $Cr_2Ti$, and γ′-phase $Ni_3(Al,Ti)$ are observed. The crystalline grain size ($D$) was calculated using Scherrer's formula:

$$D = 0.94\lambda/(\beta\cos\theta) \quad (4)$$

where $D$ represents the crystalline grain size of the alloy, m; $\beta$ is the broadening of a given diffraction line (full-width at half-maximum (FWHM)), $\lambda$ is the wavelength of incident X-rays, $1.54 \times 10^{-10}$ m; and $\theta$ is the angle of diffraction.

The crystalline grain size was evaluated for both the GTA and the PCGTA weldments. The crystalline grain size of the GTA weldment was approximately $3.67 \times 10^{-10}$ m, whereas that for the PCGTA weldment was approximately $3.52 \times 10^{-10}$ m. The results show that switching from the GTAW to the PCGTAW technique resulted in a reduction of approximately 4.01% in the percentage of crystalline grains. Thus, the PCGTAW technique refined the microstructure.

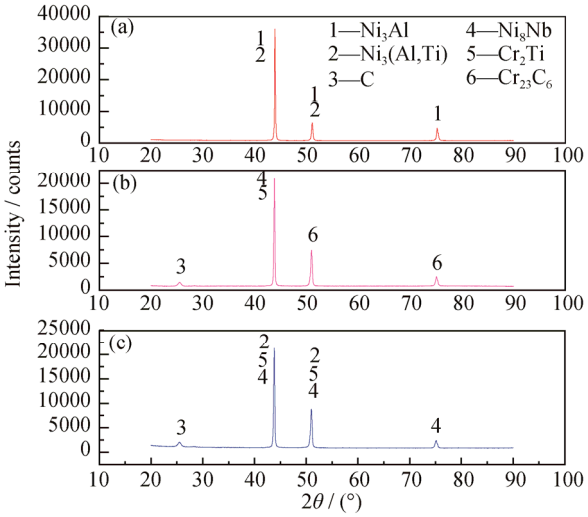


**Fig. 8. XRD analysis results for alloy 80A weld joints: (a) base metal; (b) GTA–ERNiCr-3; (c) PCGTA–ERNiCr-3.**

### 3.5. Tensile testing

Table 5 shows the ultimate tensile strength (UTS), percentage of elongation, and yield strength of the GTA and PCGTA weldments. The tensile failure samples of both GTA and PCGTA weldments are shown in Fig. 9. Fracture occurred in the FZ for both weld joints. The PCGTA weldments (Table 5) exhibit greater strength than similar GTA weldments. In addition, the strengths of both the GTA and PCGTA weldments are lower than that of the BM. Microvoids with dimples are observed in the SEM fractography (Fig. 10) of both of the tensile failure specimens.

**Table 5. Tensile test results for GTA and PCGTA weldments produced using ERNiCr-3 filler wire**

| Welding process | UTS / MPa | Average UTS / MPa | Yield strength / MPa | Average yield strength / MPa | Elongation / % | Average elongation / % | Fracture zone |
|---|---|---|---|---|---|---|---|
| Base metal | 933 | | 521.51 | | 20.1 | | |
| GTAW | 812 | 796 | 517.47 | 479.67 | 8.6 | 7.8 | Fractured at weld zone |
| | 788 | | 459.92 | | 7.9 | | |
| | 790 | | 461.64 | | 6.8 | | |
| PCGTAW | 838 | 816 | 418.06 | 426.55 | 8.5 | 8.4 | Fractured at weld zone |
| | 794 | | 435.89 | | 8.2 | | |
| | 818 | | 425.70 | | 8.5 | | |

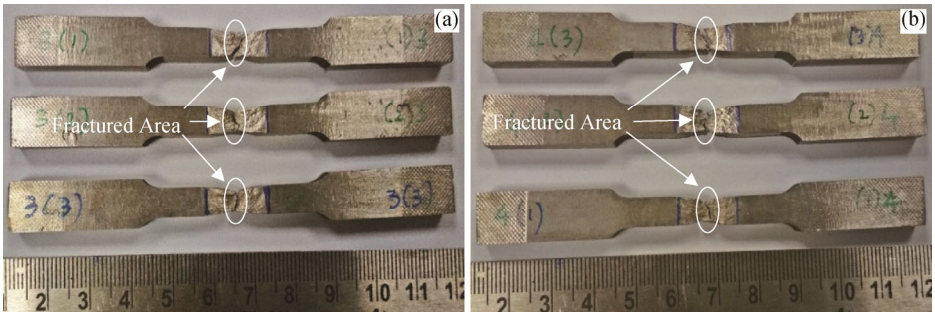


**Fig. 9. Photographs of tensile failure specimens of (a) GTA weldment and (b) PCGTA weldment produced using ERNiCr-3 filler wire.**

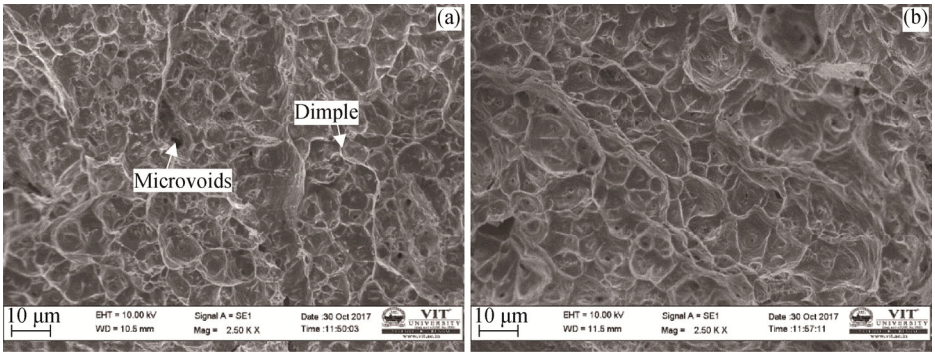


**Fig. 10. SEM fractographs of tensile failure specimens of (a) GTA weldment and (b) PCGTA weldment produced using ERNiCr-3 filler wire.**

## 4. Discussion

### 4.1. Macroscopic examination for weld quality evaluation

In the current study, the quality of the weldments was evaluated through macroscale examination. Figs. 2(a) and 2(b) shows the cross-sectional view of the GTA and PCGTA weldments fabricated with ERNiCr-3 filler wire. In general, welding occurs by transfer of thermal energy from the electrode to the weld pool through the arc plasma via convention heat transfer. The high heat produced at the center of the molten pool is dispersed to the atmosphere through the BM in the longitudinal direction. The macrographic image (Figs. 2(a) and 2(b)) shows that steady fluid flow is achieved in the pool geometry of the weldments with good morphology. The weld-pool geometry can be described through the forces (buoyancy force, Lorentz force, and shear stress force) created through the interaction of the arc plasma and the weld pool. The buoyancy force is helpful in filling the molten metal in the V-groove configuration without any defects. The Lorentz force is beneficial in increasing the depth of penetration by directing the molten fluid to flow along the axis of the weld pool. The sheer-stress force allows the molten fluid to move from the centerline of the weld pool to the weld interface for proper filling and also pushes the fluid to flow inward to increase the depth of penetration. We observed from the macrographic image, in both the case of GTAW and PCGTAW, weldments produced with ERNiCr-3 filler wire are free from defects such as porosity, cracks and any other defects. Thus, the welding technique and its corresponding process parameter adopted for joining a 6-mm-thick plate of alloy 80A are optimum. We also inferred that the FZ width of the PCGTA weldment is narrower than that of the GTA weldment. We speculate that the lower heat input of 1.809 kJ/mm achieved in the PCGTA weldment compared with the heat input of 2.052 kJ/mm achieved in the GTA weldment is responsible for the reduction in width of the weld bead. Similar observations were noted by several other researchers [18–19].

### 4.2. Microstructure examination

The procured alloy 80A was subjected to a heat treatment (1060°C for 8 h) to ensure adequate mixing of the alloying elements into the metal matrix of the alloy. Annealing twins were identified on the grain boundaries (Fig. 3). The annealing twins are the result of recrystallization of the deformed structure during the solution treatment of alloy 80A [20]. Figs. 4 and 5 show micrographic images of the GTA and PCGTA weldments produced with ERNiCr-3 filler

wire. Figs. 4(a) and 5(a) represent the FZ weld-center region, whereas Figs. 4(b) and 5(b) show the FZ weld-interface region of the GTAW and PCGTAW. Fig. 4 shows that the microstructure of the GTA weldment consisted of a cellular and columnar structure. By contrast, Fig. 5 shows the equiaxed dendritic and columnar dendritic structures in PCGTA weldment. The development of the cellular structure and columnar dendritic structures in the weld zone can be explained through the breakdown of the planar solid–liquid interface structure in the interface region by thermal gradient. Generally, extensive grain growth will occur in the weld center, where the thermal gradient is low. In addition, grain growth will be low in the fusion line because the temperature gradient is steepest at that region. The columnar dendritic structure observed in the fusion line is due to the growth of grains in the easy growth directions of <100> crystallographic plane aligned with the heat dispersion direction, which is perpendicular to that of the weld-pool region [20–21]. We also inferred that the microstructures of the GTA weldments are coarser in size compared with those of similar PCGTA weldments. The resultant coarsened microstructure is attributed to the higher heat input and slower cooling rate achieved in GTAW compared with those in PCGTAW. The higher heat input results in high temperatures, which promote the dispersion of grain [22–24]. In the PCGTA weldments, refinements of the microstructure are observed, which is speculated due to the influence of pulsing current provided during welding. In general, the cyclic variation of input energy causes thermal fluctuation in the weld pool, which leads to periodic interruptions in the solidification process. During peak current, melting of metal occurs, followed by the base current, during which solidification occurs; i.e., new grains start to grow in the weld zone. As the current increases in the subsequent cycle, the formation of new grains is arrested, and re-melting of growing grains occurs. As this cyclic process repeats, the temperature fluctuates in the weld-pool region, and it changes the shape and size of the weld pool, favoring for the growth of new grains. Thus, the rate of grain growth increases in the small distance, which enables the growth of more grains, resulting in refinement of the microstructure [21]. Similar refinement of microstructures has been noted by other researchers [14–15].

From the microstructure of the GTA weldment (Fig. 4), the existence of the solidification grain-boundaries (SGBs) is observed. The SGBs are formed by the intersection of a group of grains or packets. The SGBs promote redistribution of solute during the solidification process [25]. In the present work, Cr and Nb segregation in the interdendritic region of the FZ is observed using EDS analysis. During solidification, low-melting liquid films tend to grow along SGBs because of Cr and Nb precipitation, which in turn promotes solidification cracking [25]. However, in the present study, solidification cracking was not observed in the weld zone. A detailed analysis should be conducted in the near future.

We inferred from Figs. 4(b) and 5(b) the HAZ microstructure of GTA and PCGTA weldments. That is, in the PCGTA weldment, refinement of grains in the HAZ region is observed when the size of these grains is compared with that of the grains in the BM. By contrast, in GTA weldments, size of the grains in the HAZ region is similar to that of grains in the BM. The observed grain refinement in the HAZ region of PCGTA weldments is attributed to the confined heat input achieved in the PCGTAW. A similar observation has been reported by other researchers [12,21].

### 4.3. SEM/EDS analysis

During solidification, the development of Cr carbide precipitates and depletion of Cr around the grain boundaries promotes hot cracking in the weld zone [7]. SEM/EDS analysis is used to assess the microsegregation of alloying elements in the grain boundaries of the weldments. Figs. 6(a–b) and 7(a–b) show higher-magnification SEM images of both GTA and PCGTA weldments fabricated with ER-NiCr-3 filler wire. Figs. 6(a) and 7(a) show SEM micrographs of the weld center, and Figs. 6(b) and 7(b) show SEM micrographs of the weld-interface region of the FZ. Figs. 6(a–b) and 7(a–b) show that secondary phases are visible in the interdendritic region of the FZ. The PCGTA weldment is inferred to contain fewer secondary-phase particles than the GTA weldment. The reduction in microsegregation observed in the PCGTA weldments is due to the high cooling rate achieved during welding. The refined microstructure is the result of a higher cooling rate achieved in the PCGTA weldment. As a consequence of the refined microstructure, more grain boundaries exist. These grain boundaries result in a lower free energy, reducing the rate of precipitation of carbide around the grain boundaries [21]. Similar observations have been reported by other research groups [16–17].

EDS analysis was carried out to determine the mass percentages of elements in the grain and grain-boundary (interdendritic) region of the weld zone. The EDS analysis results are shown in Figs. 6 and 7 and are tabulated in Tables 3 and 4. The results for the GTA weldment show that Cr- and Nb-rich precipitates are present in the interdendritic region of the weld zone. By contrast, in the PCGTA weldment, on-

ly Nb-rich precipitates are observed in the interdendritic region. In general, the development of Cr carbide precipitates depends on the Cr and C contents and also on the exposure of alloy 80A to high temperatures. In GTAW, high heat is continually supplied to the molten pool, which results in high temperatures in the molten pool. The exposure of the molten pool to high temperatures for a period of time results in depletion of Cr in the grain boundaries and the segregation of Cr as precipitates in the grain boundary [26]. These segregated Cr precipitates were observed as Cr-rich precipitates by SEM and EDS analyses.

The microsegregation of Nb-rich precipitates in the grain boundary (interdendritic region) is observed in both the GTA and the PCGTA weldments. The Nb precipitates in the interdendritic region because it has a greater bonding affinity with carbon during solidification than the other alloying elements, such as Cr and Fe.

The exposure of alloy 80A to high temperatures results in the formation of $M_{23}C_6$ Cr-rich carbide precipitates around the grain boundaries, which is detrimental to the mechanical properties of alloy 80A [7,27]. SEM reveals the presence of secondary phases in both the GTA and the PCGTA weldments. The EDS analysis results show that Cr- and Nb-rich precipitates form as secondary phases in the GTA weldments. By contrast, in PCGTA weldments, only Nb precipitates form.

### 4.4. XRD analysis

XRD analysis was conducted on both weld zone and BM to characterize the presence of secondary phases in the grain boundary region. The results are displayed in Fig. 8. The EDS analysis results support the XRD analysis in the present study. The Cr- and Nb-rich precipitates observed in the GTA weldments through XRD analysis are $Cr_{23}C_6$ ($M_{23}C_6$) carbides, $Ni_8Nb$, and $Cr_2Ti$ phases. In contrast to the GTA weldments, the PCGTA weldments contained only segregated Nb, as revealed by EDS analysis; the resultant phases were found to be $Ni_8Nb$ and $Cr_2Ti$ phases.

### 4.5. Tensile tests

The strength and ductility of weldments were investigated through tensile testing; the results are shown in Table 5. The BM tensile test results are also listed in Table 5 for reference. The results in Table 5 show that the strength and ductility of the PCGTA weldments are slightly better than those of the GTA weldments. We also obseved that, in comparison with the BM, the weldments exhibit lower strength and lower ductility. The difference in the strength and ductility are attributed to the existence of secondary phases in the interdendritic region of the weld zone. The presence of embrittlement phases $Cr_{23}C_6$ ($M_{23}C_6$) carbide and $Ni_8Nb$ in the interdendritic region are responsible for the decrease in the strength and ductility of the weldment compared with those of the BM [28–29].

We also noted that the UTS of the GTA weldment is slightly lower than that of the PCGTA weldment. This slight decrease in strength is due to greater Cr segregation in the GTA weldment. In the case of the PCGTA weldment, the loss in strength compared with that of the BM is due to segregation of a substantial amount of $Ni_8Nb$ phase in the interdendritic region, as observed in the EDS and XRD analyses. Feng *et al.* [29] stated that the presence of the $Ni_8Nb$ phase tended to adversely affect the mechanical properties of alloy 718. Our results indicate that the strength of the PCGTA weldments is slightly greater than that of the GTA weldments. This difference in strength is due to the existence of a strengthening phase ($\gamma'$), $Ni_3(Al,Ti)$, and the refinement of the crystalline grain size. We calculated an approximate 4.01% reduction in the crystalline grain size in the PCGTA weldment compared with that in the GTA weldment. The refinement of crystalline grain size in the PCGTA weldment tends to increase the strength and ductility of the weld joint compared with those of the GTA weldment [30]. We also inferred that the percentages of elongation of the weldments are lower than that of the BM. The poor elongation observed in the weldments is due to the existence of the $Cr_2Ti$ phase, which was detected by XRD analysis. Wang *et al.* [31] found that the $Cr_2Ti$ phase, which they also detected through XRD, was responsible for the poor plasticity observed in the alloy Ti6.0Al4.5Cr1.5Mn. Fig. 9 shows photographs of tensile failure samples of GTA and PCGTA weldments. These photographs reveal that fracture occurred in the weld zone for both the GTA and PCGTA weldments. SEM fractographs of the tensile failure specimens of the weldments are shown in Fig. 10. The SEM fractographs were used to judge the mode of failure in the tensile specimens. The observed microvoids and dimples in the SEM factographs indicate ductile failure occurred in both GTA and PCGTA weldments.

### 4.6. Recommendations

In the present work, between the two weldments fabricated using ERNiCr-3 filler wire, the PCGTA weldment showed better results. Adaptation of the PCGTAW technique resulted in (1) a refined microstructure, (2) complete eradication of Cr carbide precipites from the grain boundaries, and (3) better strength and ductility compared with those of GTA weldments.

## 5. Conclusions

(1) Defect-free weldments were produced using both GTAW and PCGTAW techniques, which confirms that an appropriate welding technique, filler wire, and process parameters were selected. The confined heat input resulted in a narrower bead width in the PCGTA weldments.

(2) In the case of PCGTA weldments fabricated with ERNiCr-3 wire, equiaxed dendritic structures were detected at the FZ weld center. By contrast, in GTA weldments, a coarser microstructure was observed. The observed refined microstructure was largely due to a faster cooling rate achieved through the PCGTAW technique.

(3) Secondary phases were identified in the weld zones for both GTA and PCGTA weldments. In the case of GTA weldment, the precipitation of Cr and Nb was observed. By contrast, in the PCGTA weldment, Nb-rich precipitates were identified. Also, the PCGTA weldment exhibited less segregation of alloying elements along with the complete suppression of Cr carbide precipitates during solidification when compared to GTA weldment.

(4) In GTA weldments, $Cr_{23}C_6$ ($M_{23}C_6$), $Ni_8Nb$, and $Cr_2Ti$ phases were observed. By contrast, in PCGTA weldments, $Ni_8Nb$, $Cr_2Ti$, and $Ni_3(Al,Ti)$ phases were identified.

(5) PCGTA weldments exhibited slightly greater strength and ductility than GTA weldments. The refinement in the crystalline grain size and a smaller volume of segregation were responsible for the better mechanical properties of the PCGTA weldments.

## Acknowledgements

The authors thank Mr. Natarajan R, Delta Wearteach Engineers Pvt. Ltd. for his welding support and thank to Dr. Narendra Kumar, Vellore Institute of Technology, for helping the microstructural analysis. We also thank to Department of Science and Technology, Government of India, for supporting the SEM and INSTRON universal testing machine facility established at Vellore Institute of Technology utilized for this research work.

## References

[1] V. Sreenivasulu and M. Manikandan, High-temperature corrosion behaviour of air plasma sprayed $Cr_3C_2$–25NiCr and NiCrMoNb powder coating on alloy 80A at 900°C, *Surf. Coat. Technol.*, 337(2018), p. 250.

[2] N. Swain, P. Kumar, G. Srinivas, S. Ravishankar, and H.C. Barshilia, Mechanical micro-drilling of Nimonic 80A superalloy using uncoated and TiAlN-coated micro-drills, *Mater. Manuf. Processes*, 32(2017), No. 13, p. 1537.

[3] A. D. Gianfrancesco, *Materials for Ultra-Supercritical and Advanced Ultra-Supercritical Power Plants*, Woodhead Publishing, Cambridge, 2017, p. 186.

[4] W.E. Voice and R.G. Faulkner, Carbide stability in Nimonic 80A alloy, *Metall. Trans. A*, 16(1985), No. 4, p. 511.

[5] D. Bombac, M. Brojan, M. Tercelj, and R. Turk, Response to hot deformation conditions and microstructure development of Nimonic 80A superalloy, *Mater. Manuf. Processes*, 24(2009), p. 644.

[6] K.H. Keienburg, W. Eßber, and B. Deblon, Refurbishing procedures for blades of large stationary gas turbines, *Mater. Sci. Technol.*, 1(1985), No. 8, p. 620.

[7] S. Kargarnejad and F. Djavanroodi, Failure assessment of Nimonic 80A gas turbine blade, *Eng. Fail. Anal*., 26(2012), p. 211.

[8] M. Gao and R.P. Wei, Precipitation of intragranular $M_{23}C_6$ carbides in a nickel alloy: Morphology and crystallographic features, *Scripta Metall.*, 30(1994), No. 8, p. 1009.

[9] Y.L. Xu, C.X. Yang, Q.X. Ran, P.F. Hu, X.S. Xiao, X.L. Cao, and G.Q. Jia, Microstructure evolution and stress-rupture properties of Nimonic 80A after various heat treatments, *Mater. Des.*, 47(2014), p. 218.

[10] *VDM® Alloy 80 A*, Material data sheet No. 4048, VDM Metals International GmbH, 2017. https://www.vdm-metals.com/fileadmin/user_upload/Downloads/Data_Sheets/Data_Sheet_VDM_Alloy_80_A.pdf

[11] G.D.J. Ram, A.V. Reddy, K.P. Rao and G.M. Reddy, Control of Laves phase in Inconel 718 GTA welds with current pulsing, *Sci. Technol. Weld. Joining*, 9(2004). No. 5, p. 390.

[12] S.G.K. Manikandan, D. Sivakumar, K.P. Rao, and M. Kamaraj, Effect of weld cooling rate on Laves phase formation in Inconel 718 fusion zone, *J. Mater. Process. Technol.*, 214(2014), No. 2, p. 358.

[13] B. Arulmurugan and M. Manikandan, Development of welding technology for improving the metallurgical and mechanical properties of 21st century nickel based superalloy 686, *Mater. Sci. Eng. A*, 691(2017), p. 126.

[14] M. Manikandan, N. Arivazhagan, M.N. Rao, and G.M. Reddy, Microstructure and mechanical properties of alloy C-276 weldments fabricated by continuous and pulsed current gas tungsten arc welding techniques, *J. Manuf. Processes*, 16(2014), No. 4, p. 563.

[15] M. Manikandan, N. Arivazhagan, M.N. Rao, and G.M. Reddy, Improvement of microstructure and mechanical behavior of gas tungsten arc weldments of alloy C-276 by current pulsing, *Acta Metall Sin Engl. Lett.*, 28(2015), No. 2, p. 208.

[16] K.D. Ramkumar, S.R. Krishnan, R. Ramanand, S. Logesh, T. Satyandas, A. Ameer, and N. Arivazhagan, Structure–property relationships of PCGTA welds of Inconel X750 in as-welded and post-weld heat treated conditions—A comparative study, *J. Manuf. Processes*, 20(2015), p. 1.

[17] A. Srikanth and M. Manikandan, Development of welding technique to avoid the sensitization in the alloy 600 by conventional Gas Tungsten Arc Welding method, *J. Manuf. Processes*, 30(2017), p. 452.

[18] T. Pasang, J.M.S. Amaya, Y. Tao, M.R. Amaya-Vazquez, F.J. Botana, J.C. Sabol, W.Z. Misiolek, and O. Kamiya, Comparison of Ti–5Al–5V–5Mo–3Cr welds performed by laser beam, electron beam and gas tungsten arc welding, *Procedia Eng.*, 63(2013), p. 397.

[19] K.Y. Benyounis, A.G. Olabi, and M.S.J. Hashmi, Effect of laser welding parameters on the heat input and weld-bead profile, *J. Mater. Process. Technol.*, 164-165(2005), p. 978.

[20] S.A. David, S.S. Babu, and J.M. Vitek, Welding: Solidification and microstructure, *JOM*, 55(2003), No. 6, p. 14.

[21] E. Farahani, M. Shamanian, and F. Ashrafizadeh, A comparative study on direct and pulsed current gas tungsten arc welding of alloy 617, *AMAE Int. J. Manuf. Mater. Sci.*, 2(2012), No. 1, p. 1.

[22] G.F.V. Voort, *ASM Handbook Volume 9: Metallography and Microstructures*, ASM International, Materials Park, Ohio, 2004.

[23] D. Peng, J. Shen, Q. Tang, C.P. Wu, and Y.B. Zhou, Effects of aging treatment and heat input on the microstructures and mechanical properties of TIG-welded 6061-T6 alloy joints, *Int. J. Miner. Metall. Mater.*, 20(2013), No. 3, p. 259.

[24] H.T. Liu, J.X. Zhou, D.Q. Zhao, Y.T. Liu, J.H. Wu, Y.S. Yang, B.C. Ma, and H.H. Zhuang, Characteristics of AZ31 Mg alloy joint using automatic TIG welding, *Int. J. Miner. Metall. Mater.*, 24(2017), No. 1, p. 102.

[25] N.J. Dupoint, C.J. Lippold, and D.S. Kiser, *Welding Metallurgy and Weldability of Nickel-Base Alloys*, John Wiley & Sons, Inc., Hoboken, New Jersey, 2009.

[26] Y.S. Sato, P. Arkom, H. Kokawa, T.W. Nelson, and R.J. Steel, Effect of microstructure on properties of friction stir welded Inconal Alloy 600, *Mater. Sci. Eng. A*, 477(2008), No. 1-2, p. 250.

[27] J.M. Donachie and J.S. Donachie, *Superalloys: A Technical Guide*, 2nd ed., ASM International, Materials Park, Ohio, 2002.

[28] K. Tamaki, H. Kawakami, M. Kojima, Y. Akazaki, and K. Nomoto, Influence of metallurgical factors on temper embrittlement in HAZ of Cr–Mo steel, *Res. Rep. Fac. Eng. Mie Univ.*, 22(1997), p. 11.

[29] K.Y. Feng, P. Liu, H.X. Li, S.Y. Sun, S.B. Xu, and J.N. Li, Microstructure and phase transformation on the surface of Inconel 718 alloys fabricated by SLM under 1050°C solid solution + double ageing, *Vacuum*, 145(2017), p. 112.

[30] W.D. Callister and D.G. Rethwisch, *Materials Science and Engineering*, 2nd ed., John Wiley and Sons, Inc., Hoboken, New Jersey, 2014.

[31] H.B. Wang, S.S. Wang, P.Y. Gao, T. Jiang, X.G. Lu, and C.H. Li, Microstructure and mechanical properties of a novel near-α titanium alloy Ti6.0Al4.5Cr1.5Mn, *Mater. Sci. Eng. A*, 672(2016), p. 170.